International Journal of Heat and Mass Transfer 67 (2013) 768–775

Contents lists available at ScienceDirect

International Journal of Heat and Mass Transfer

journal homepage: www.elsevier.com/locate/ijhmt

Analysis of thermally developing flow in porous media under local thermal non-equilibrium conditions

Xiao-Long Ouyang [a,b], Kambiz Vafai [b,*], Pei-Xue Jiang [a]

[a] Key Laboratory of CO_2 Utilization and Reduction Technology, Department of Thermal Engineering, Tsinghua University, Beijing 100084, China
[b] Department of Mechanical Engineering, University of California, Riverside, CA 92521-0425, USA

ARTICLE INFO

Article history:
Received 18 July 2013
Received in revised form 19 August 2013
Accepted 21 August 2013

Keywords:
Local thermal non-equilibrium
Thermally developing
Porous media
Analytical solution

ABSTRACT

In the present study, analytical solutions for thermally developing flows in porous media under local thermal non-equilibrium (LTNE) condition are derived for different fundamental models. The analytical solutions are validated by comparison with the numerical results. Based on the analytical solutions, the local Nusselt number is obtained, and the dimensionless thermal entry length ξ_c is predicted. The results are presented in terms of the pertinent physical parameters such as the Biot number and the effective thermal conductivity ratio of the fluid to solid phases.

1. Introduction

Thermally developing section usually has a larger heat transfer capacity than the corresponding thermally fully developed section in a confined channel flow since it is dominated by the thermal boundary effect. The thermal development problem for a laminar flow in a tube was investigated by Graetz [1]. In a channel fully filled with a porous medium, the thermally developing section can also play a significant role. Two characteristics appear due to the existence of a porous medium. First, in contrast to the case without a porous medium, the momentum boundary layer thickness is confined to a region of the order of $\sqrt{K/\varepsilon}$ and the flow boundary effect is less important in most cases in the presence of a porous medium, as pointed out by Vafai and Tien [2]. Second, the local temperature difference between the solid and fluid phases can substantially influence the heat transfer process.

There are two primary ways to model the heat transfer process in porous media: the local thermal equilibrium (LTE) model and the local thermal non-equilibrium (LTNE) model. In the LTE model the interphase temperature difference is neglected, while the LTNE model accounts for the interphase temperature differences. Early investigations have focused more on the LTE model coupled with non-Darcian effects. Vafai and Tien [2] analyzed the forced convection in porous media with the LTE model and discussed the non-Darcian effects on temperature and Nusselt number. For the confined channel flow in porous media, Haji-Sheikh and Vafai [3] and Haji-Sheikh et al. [4] derived the analytical solutions of thermally developing flows in porous media.

Amiri and Vafai [5] analyzed the dispersion effects, non-Darcian effects, variable porosity and the LTNE effects for flow through porous media. They presented error maps to establish conditions under which LTE model can be utilized. Jiang et al. [6,7] investigated the convection heat transfer in channels filled with packed particles or sintered porous media using the LTNE and LTE models, and compared their results with experiments [8,9]. They found good agreement between the LTNE model and the experimental results while the LTE model did not match with their data. Nield and Kuznetsov [10] presented a semi-analytical solution of thermally developing flow in a porous medium using the LTNE model, but no explicit expression was presented. The first analytical solution for the thermal developing region in porous media while incorporating LTNE model condition was derived by Yang and Vafai [11] for an isothermal wall boundary condition.

In this work, we will visit the work analyzed by Yang and Vafai [11] under constant heat flux boundary condition. The constant wall heat flux boundary condition is quite involved when incorporating the LTNE aspects, as introduced by Alazmi and Vafai [12] and Ouyang et al. [13].

The analysis for thermally fully developed flow while incorporating the LTNE conditions with an imposed constant wall heat flux has been established. Lee and Vafai [14] studied analytically the thermally fully developed region of a channel with an imposed constant heat flux condition, based on the LTNE and LTE models.

* Corresponding author. Tel.: +1 951 827 2135; fax: +1 951 827 2899.
E-mail address: vafai@engr.ucr.edu (K. Vafai).

0017-9310/$ - see front matter © 2013 Elsevier Ltd. All rights reserved.
http://dx.doi.org/10.1016/j.ijheatmasstransfer.2013.08.056

Nomenclature

Bi	$\mathrm{Bi}=\frac{\alpha h_{sf} H^2}{k_{s,eff}}$, Biot number
c_p	heat capacity [J/kg K]
h_{fs}	interfacial heat transfer coefficient [W/m^2 K]
H	half of the height of the channel [m]
$j_{m,n}$	dimensionless parameter defined by Eq. (18)
k	thermal conductivity [W/m K]
K	permeability [m^2]
Nu	Nussult number
Pe	$\mathrm{Pe}=\frac{\rho_f c_{pf} u H}{k_{f,eff}}$, Pectlet number
q_w	wall heat flux [W/m^2]
T	temperature [K]
T_{f0}	inlet fluid temperature [K]
u	Darcy velocity [m/s]
x	axial coordinate [m]
y	transverse coordinate [m]

Greek symbols

α	phase interface area per unit volume [m^{-1}]
γ_m	$\gamma_m = (1+\kappa)[(0.5+m)^2\pi^2+\lambda^2]$
Δ	dimensionless temperature difference defined by Eq. (12)
ε	volume fraction
η	$\eta=\frac{y}{H}$, dimensionless transverse coordinate
κ	$\kappa=\frac{k_{f,eff}}{k_{s,eff}}$, effective thermal conductivity ratio of the fluid to solid phases
λ	$\lambda=\sqrt{\mathrm{Bi}(1+\kappa)/\kappa}$, dimensionless parameter
ρ	density [kg/m^3]
σ_n	$\sigma_n=\frac{1+K}{\kappa}(n\pi)^2$, dimensionless parameter
θ	$\frac{(T-T_{f0})k_{s,eff}}{q_w H}$, dimensionless temperature
θ_a	dimensionless averaged temperature defined by Eq. (12)
ω	dimensionless decay factor for thermally developing component
ξ	$\xi=\frac{x}{PeH}$, dimensionless axial coordinate

Subscripts

A,B,C	Models A, B and C
c	the transition point where the thermally developing flow transits to the thermally fully developed flow
eff	effective
f	fluid phase
LTE	the LTE model
s	solid phase

They found that the Biot number, Bi and the effective thermal conductivity ratio, κ are the key parameters for the validity of LTE model and had presented an error map establishing the validity region of the LTE model in terms of Bi and κ. The phenomenon of heat flux bifurcation was introduced by Yang and Vafai [11,15–17]. In the present work, the corresponding theory for the thermally developing flow is analyzed, especially the transition point where the thermally developing flow transits to the thermally fully developed flow in a channel filled with a porous medium. In the present work, analytical solutions are established and the transition point is predicted.

2. Modeling and formulation

Convective transport through a channel filled with a porous medium is considered, as shown in Fig. 1. Only the upper half of the channel is considered due to the symmetry. A fluid at T_{f0} flows through the channel and each wall of the channel receives a constant heat flux q_w. Thus, the thermal boundary layers develop along the axial coordinate until x reaches the transition point $x = x_c$. The portion of channel with $x < x_c$, i.e., the thermally developing section is the focus of the current study. The value of x_c represents the thermal entry length. The following assumptions are adopted in the present study:

(1) The flow is steady and incompressible and can be represented by the Darcy flow model.
(2) Axial conduction is neglected in the governing equations.
(3) Natural convection and radiative heat transfer are negligible.
(3) Properties such as porosity, specific heat, density and thermal conductivity are assumed to be constant.

Based on these assumptions, the following energy equations are obtained from Amiri and Vafai [5] employing the LTNE model:

$$\begin{cases} \rho_f c_{pf} u \frac{\partial T_f}{\partial x} = k_{f,eff} \frac{\partial^2 T_f}{\partial y^2} + a h_{sf}(T_s - T_f) \\ 0 = k_{s,eff} \frac{\partial^2 T_s}{\partial y^2} + a h_{sf}(T_f - T_s) \end{cases} \quad (1)$$

where T_f and T_s denote the fluid and solid temperatures, $k_{f,eff}$ and $k_{s,eff}$ the effective fluid and solid conductivities, and u the Darcy velocity.

For the boundary conditions at the heated wall with constant heat flux, the following three models are considered, which are introduced by Amiri and Vafai [18]. These models are based on different assumptions.

Model A: The wall temperature of each phase at the wall is considered to be equal to each other.

$$T_f = T_s, \quad -k_{f,eff}\frac{\partial T_f}{\partial y} - k_{s,eff}\frac{\partial T_s}{\partial y} = q_w \text{ at } y = 0 \quad (2)$$

Model B: Each phase is considered to receive the same imposed heat flux at the wall.

$$-k_{f,eff}\frac{\partial T_f}{\partial y} = -k_{s,eff}\frac{\partial T_s}{\partial y} = q_w \text{ at } y = 0 \quad (3)$$

Model C: The intrinsic averaged wall heat fluxes of the two phases are considered to be equal.

$$-\frac{k_{f,eff}}{\varepsilon}\frac{\partial T_f}{\partial y} = -\frac{k_{s,eff}}{1-\varepsilon}\frac{\partial T_s}{\partial y} = q_w \text{ at } y = 0 \quad (4)$$

The other boundary conditions at the central line and inlet can be presented as:

$$\begin{cases} \frac{\partial T_f}{\partial y} = \frac{\partial T_s}{\partial y} = 0 & \text{at } y = H \\ T_f = T_{f0} & \text{at } x = 0 \end{cases} \quad (5)$$

2.1. Normalization

The following non-dimensional variables have been introduced:

$$\theta = \frac{(T-T_{f0})k_{s,eff}}{q_w H}, \quad \mathrm{Bi} = \frac{a h_{sf} H^2}{k_{s,eff}}, \quad \kappa = \frac{k_{f,eff}}{k_{s,eff}},$$
$$\eta = \frac{y}{H}, \quad \xi = \frac{x}{PeH}, \quad Pe = \frac{\rho_f c_{pf} u H}{k_{f,eff}} \quad (6)$$

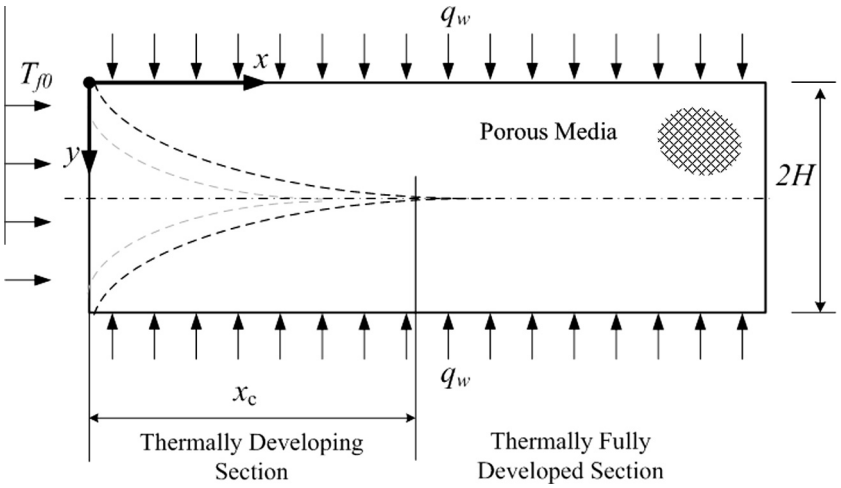

Fig. 1. Schematic diagram for a thermally developing flow through a channel filled with a porous medium and the corresponding coordinate system.

The governing equations and boundary conditions, Eqs. (1)–(5), can then be written as:

$$\begin{cases} \kappa \frac{\partial \theta_f}{\partial \xi} = \kappa \frac{\partial^2 \theta_f}{\partial \eta^2} + \mathrm{Bi}(\theta_s - \theta_f) \\ 0 = \frac{\partial^2 \theta_s}{\partial \eta^2} + \mathrm{Bi}(\theta_f - \theta_s) \end{cases} \tag{7}$$

Model A:

$$\theta_f = \theta_s, \quad -\kappa \frac{\partial \theta_f}{\partial \eta} - \frac{\partial \theta_s}{\partial \eta} = 1 \quad \text{at } \eta = 0 \tag{8}$$

Model B:

$$-\kappa \frac{\partial \theta_f}{\partial \eta} = -\frac{\partial \theta_s}{\partial \eta} = 1 \quad \text{at } \eta = 0 \tag{9}$$

Model C:

$$-\kappa \frac{\partial \theta_f}{\partial \eta} = \varepsilon, \quad -\frac{\partial \theta_s}{\partial \eta} = 1 - \varepsilon \quad \text{at } \eta = 0 \tag{10}$$

Other boundary conditions:

$$\begin{cases} \frac{\partial \theta_f}{\partial \eta} = \frac{\partial \theta_s}{\partial \eta} = 0 & \text{at } \eta = 1 \\ \theta_f = 0 & \text{at } \xi = 0 \end{cases} \tag{11}$$

3. Analysis

The following linear transformation is utilized to recast the dimensionless temperatures

$$\begin{cases} \theta_a = \frac{\theta_s + \kappa \theta_f}{1+\kappa} \\ \Delta = \theta_s - \theta_f \end{cases}, \quad \begin{cases} \theta_f = \theta_a - \frac{\Delta}{1+\kappa} \\ \theta_s = \theta_a + \frac{\kappa \Delta}{1+\kappa} \end{cases} \tag{12}$$

where θ_a denotes the dimensionless local averaged temperature weighed by effective conductivities, and Δ the dimensionless local temperature difference. These two variables are also important for the subsequent analysis.

3.1. Analytical solution for Model A

The analytical solution for Model A has to incorporate the fact that the temperature variables are coupled with the boundary condition given by Eq. (8). Applying the transformation given by Eq. (12), the governing equations given in Eq. (7) can be represented as

$$\begin{cases} \frac{\partial \theta_a}{\partial \xi} = \frac{1+\kappa}{\kappa} \frac{\partial^2 \theta_a}{\partial \eta^2} + \frac{1}{1+\kappa} \frac{\partial \Delta}{\partial \xi} \\ \frac{1}{1+\kappa} \frac{\partial \Delta}{\partial \xi} = \frac{\partial^2 \Delta}{\partial \eta^2} - \mathrm{Bi} \frac{1+\kappa}{\kappa} \Delta + \frac{\partial \theta_a}{\partial \xi} \end{cases} \tag{13}$$

while the boundary conditions given by Eqs. (8) and (11) become

$$\begin{cases} -(1+\kappa) \frac{\partial \theta_a}{\partial \eta} = 1, \quad \Delta = 0 & \text{at } \eta = 0 \\ \frac{\partial \theta_a}{\partial \eta} = \frac{\partial \Delta}{\partial \eta} = 0 & \text{at } \eta = 1 \\ \theta_a = \Delta = 0 & \text{at } \xi = 0 \end{cases} \tag{14}$$

A series distribution utilized for θ_a and Δ as given below

$$\begin{cases} \theta_a = \frac{1}{1+\kappa} \left[\frac{a_{\theta,0}(\xi)}{\sqrt{2}} + \sum_{n=1}^{\infty} a_{\theta,n}(\xi) \cos(n\pi\eta) \right] \\ \Delta = \sum_{m=0}^{\infty} a_{\Delta,m}(\xi) \sin((0.5+m)\pi\eta) \end{cases} \tag{15}$$

Integrating Eq. (13) with respect to η after multiplying it by $\cos(n\pi\eta)$ or $\sin((0.5+m)\pi\eta)$ results

$$\begin{cases} \frac{da_{\theta,0}}{d\xi} = \sqrt{2} \frac{1+\kappa}{\kappa} + \sum_{m=0}^{\infty} j_{m,0} \frac{da_{\Delta,m}}{d\xi}, \quad n = 0 \\ \frac{da_{\theta,n}}{d\xi} = 2 \frac{1+\kappa}{\kappa} - \sigma_n a_{\theta,n} + \sum_{m=0}^{\infty} j_{m,n} \frac{da_{\Delta,m}}{d\xi}, \quad n = 1,2,3,\ldots \\ \frac{da_{\Delta,m}}{d\xi} = -\gamma_m a_{\Delta,m} + \sum_{n=0}^{\infty} j_{m,n} \frac{da_{\theta,n}}{d\xi}, \quad m = 0,1,2,\ldots \end{cases} \tag{16}$$

where

$$\sigma_n = \frac{1+\kappa}{\kappa}(n\pi)^2, \quad \gamma_m = (1+\kappa)\left[(0.5+m)^2\pi^2 + \lambda^2\right], \quad \lambda = \sqrt{\mathrm{Bi}(1+\kappa)/\kappa} \tag{17}$$

$$j_{m,n} = \begin{cases} \sqrt{2} \int_0^1 \sin((0.5+m)\pi\eta) d\eta = \frac{\sqrt{2}}{\pi} \frac{1}{0.5+m}, & n = 0 \\ 2 \int_0^1 \sin((0.5+m)\pi\eta) \cos(n\pi\eta) d\eta = \frac{2}{\pi} \frac{0.5+m}{(0.5+m)^2 - n^2}, & n = 1,2,3,\ldots \end{cases} \tag{18}$$

and $j_{m,n}$ is a special set with the following orthogonality characteristic

$$\sum_{n=0}^{\infty} j_{m,n} j_{k,n} = \begin{cases} 1, & m = k \\ 0, & m \neq k \end{cases}, \quad \sum_{m=0}^{\infty} j_{m,n} j_{m,k} = \begin{cases} 1, & n = k \\ 0, & n \neq k \end{cases} \tag{19}$$

Defining the infinite vectors:

$$\mathbf{a}_\theta(\xi)=\begin{bmatrix}a_{\theta,0}\\ a_{\theta,1}\\ a_{\theta,2}\\ \vdots\\ a_{\theta,n}\end{bmatrix},\quad \mathbf{a}_\Delta(\xi)=\begin{bmatrix}a_{\Delta,0}\\ a_{\Delta,1}\\ a_{\Delta,2}\\ \vdots\\ a_{\Delta,m}\end{bmatrix},\quad \mathbf{b}=\frac{1+\kappa}{\kappa}\begin{bmatrix}\sqrt{2}\\ 2\\ 2\\ \vdots\\ 2\end{bmatrix},$$
$$\mathbf{f}_\theta(\eta)=\begin{bmatrix}\sqrt{2}/2\\ \cos(\pi\eta)\\ \cos(2\pi\eta)\\ \vdots\\ \cos(n\pi\eta)\end{bmatrix},\quad \mathbf{f}_\Delta(\eta)=\begin{bmatrix}\sin(0.5\pi\eta)\\ \sin(1.5\pi\eta)\\ \sin(2.5\pi\eta)\\ \vdots\\ \sin((0.5+m)\pi\eta)\end{bmatrix},\quad m=n=0,1,2,\ldots \tag{20}$$

as well as defining the infinite matrices:

$$\mathbf{J}=\begin{bmatrix}j_{0,0}&j_{0,1}&\cdots&j_{0,n}\\ j_{1,0}&j_{1,1}&\cdots&j_{1,n}\\ \vdots&\vdots&\ddots&\vdots\\ j_{m,0}&j_{m,1}&\cdots&j_{m,n}\end{bmatrix},\quad \mathbf{D}(w_n)=\begin{bmatrix}w_0&0&\cdots&0\\ 0&w_1&\cdots&0\\ \vdots&\vdots&\ddots&\vdots\\ 0&0&\cdots&w_n\end{bmatrix},m=n=0,1,2,\ldots \tag{21}$$

where $\mathbf{J}$ is an orthogonal matrix due to Eq. (19)

$$\mathbf{J}\mathbf{J}^{\mathbf{T}}=\mathbf{J}^{\mathbf{T}}\mathbf{J}=\mathbf{I} \tag{22}$$

while $\mathbf{D}(w_n)$ denotes the diagonal matrix of an infinite series w_n.

As such Eq. (16) can be simplified to

$$\begin{cases}\frac{d\mathbf{a}_\theta}{d\xi}=\mathbf{b}-\mathbf{D}(\sigma_n)\mathbf{a}_\theta+\mathbf{J}^{\mathrm{T}}\frac{d\mathbf{a}_\Delta}{d\xi}\\ \frac{d\mathbf{a}_\Delta}{d\xi}=-\mathbf{D}(\gamma_m)\mathbf{a}_\Delta+\mathbf{J}\frac{d\mathbf{a}_\theta}{d\xi}\end{cases} \tag{23}$$

Eq. (23) cannot be solved directly because $\mathbf{D}(\sigma_n)$ is a singular matrix. This problem can be solved by using the Laplace transformation with respect to ξ:

$$\begin{cases}\mathbf{D}(s+\sigma_n)\mathcal{L}\{\mathbf{a}_\theta\}=\frac{\mathbf{b}}{s}+s\mathbf{J}^{\mathbf{T}}\mathcal{L}\{\mathbf{a}_\Delta\}\\ \mathbf{D}(s+\gamma_m)\mathcal{L}\{\mathbf{a}_\Delta\}=s\mathbf{J}\mathcal{L}\{\mathbf{a}_\theta\}\end{cases} \tag{24}$$

Thus, after solving Eq. (24), the exact solution can be expressed as

$$\begin{cases}\theta_a=\frac{\mathbf{a}_\theta(\xi)\cdot\mathbf{f}_\theta(\eta)}{1+\kappa}\\ \Delta=\mathbf{a}_\Delta(\xi)\cdot\mathbf{f}_\Delta(\eta)\end{cases} \tag{25}$$

where

$$\begin{cases}\mathbf{a}_\theta(\xi)=\mathcal{L}^{-1}\left\{\mathbf{U}_\theta^{-1}\frac{\mathbf{b}}{s^2}\right\}\\ \mathbf{a}_\Delta(\xi)=\mathcal{L}^{-1}\left\{\mathbf{U}_\Delta^{-1}\mathbf{J}\mathbf{D}\left(\frac{s}{s+\sigma_n}\right)\frac{\mathbf{b}}{s^2}\right\}\end{cases} \tag{26}$$

$$\begin{aligned}\mathbf{U}_\theta&=\mathbf{D}\left(\frac{s+\sigma_n}{s}\right)-\mathbf{J}^{\mathbf{T}}\mathbf{D}\left(\frac{s}{s+\gamma_m}\right)\mathbf{J}\\ \mathbf{U}_\Delta&=\mathbf{D}\left(\frac{s+\gamma_m}{s}\right)-\mathbf{J}\mathbf{D}\left(\frac{s}{s+\sigma_n}\right)\mathbf{J}^{\mathbf{T}}\end{aligned} \tag{27}$$

However, it is very difficult to obtain the exact expressions for $\mathbf{U}_\theta^{-1}$ and $\mathbf{U}_\Delta^{-1}$. Therefore, no explicit exact solution for this problem can be found here.

3.2. Approximate solution for Model A

We obtain an approximate solution by dropping a few higher ordered components in Eqs. (26) and (27). That is

$$\begin{aligned}\mathbf{U}_\theta&=\mathbf{D}\left(\frac{s+\sigma_n}{s}\right)-\frac{s}{s+\gamma_0}[j_{0,n}][j_{0,n}]^{\mathbf{T}}-\frac{s}{s+\gamma_1}[j_{1,n}][j_{1,n}]^{\mathbf{T}}\\ &-\ldots\approx\mathbf{D}\left(\frac{s+\sigma_n}{s}\right)-\frac{s}{s+\gamma_0}\begin{bmatrix}j_{0,0}^2&j_{0,0}j_{0,1}&0&\cdots&0\\ j_{0,0}j_{0,1}&j_{0,1}^2&0&\cdots&0\\ 0&0&0&\cdots&0\\ \vdots&\vdots&\vdots&\ddots&\vdots\\ 0&0&0&\cdots&0\end{bmatrix}\\ &-\frac{s}{s+\gamma_1}\begin{bmatrix}j_{1,0}^2&j_{1,0}j_{1,1}&0&\cdots&0\\ j_{1,0}j_{1,1}&j_{1,1}^2&0&\cdots&0\\ 0&0&0&\cdots&0\\ \vdots&\vdots&\vdots&\ddots&\vdots\\ 0&0&0&\cdots&0\end{bmatrix}\end{aligned} \tag{28}$$

$$\begin{aligned}\mathbf{U}_\Delta&=\mathbf{D}\left(\frac{s+\gamma_m}{s}\right)-\frac{s}{s+\sigma_0}[j_{m,0}][j_{m,0}]^{\mathbf{T}}-\frac{s}{s+\sigma_1}[j_{m,1}][j_{m,1}]^{\mathbf{T}}\\ &-\ldots\approx\mathbf{D}\left(\frac{s+\gamma_m}{s}\right)-\frac{s}{s+\sigma_0}\begin{bmatrix}j_{0,0}^2&j_{0,0}j_{1,0}&0&\cdots&0\\ j_{0,0}j_{1,0}&j_{1,0}^2&0&\cdots&0\\ 0&0&0&\cdots&0\\ \vdots&\vdots&\vdots&\ddots&\vdots\\ 0&0&0&\cdots&0\end{bmatrix}\\ &-\frac{s}{s+\sigma_1}\begin{bmatrix}j_{0,1}^2&j_{0,1}j_{1,1}&0&\cdots&0\\ j_{0,1}j_{1,1}&j_{1,1}^2&0&\cdots&0\\ 0&0&0&\cdots&0\\ \vdots&\vdots&\vdots&\ddots&\vdots\\ 0&0&0&\cdots&0\end{bmatrix}\end{aligned} \tag{29}$$

$$\begin{cases}\mathbf{a}_\theta(\xi)=\mathcal{L}^{-1}\left\{\mathbf{U}_\theta^{-1}\frac{\mathbf{b}}{s^2}\right\}\\ \mathbf{a}_\Delta(\xi)\approx\mathcal{L}^{-1}\left\{\frac{\mathbf{U}_\Delta^{-1}}{s}\left(\frac{b_0}{s+\sigma_0}[j_{m,0}]+\frac{b_1}{s+\sigma_1}[j_{m,1}]\right)\right\}\end{cases} \tag{30}$$

where $[w_n]$ denotes the column vector of an infinite series w_n. This leads to

$$\begin{cases}\theta_a=\underbrace{\frac{\xi}{\kappa}+\frac{(1-\eta)^2-1/3}{2(1+\kappa)}+\frac{j_{0,0}^2}{\kappa\gamma_0}+\frac{j_{1,0}^2}{\kappa\gamma_1}}_{\text{Fully developed component}}\\ \quad -D_1\exp(-\omega_{A0}\xi)-D_2\exp(-\omega_{A1}\xi)\\ \quad -[D_3\exp(-\omega_{A0}\xi)+D_4\exp(-\omega_{A1}\xi)]\cos(\pi\eta)\\ \quad \underbrace{-\sum_{n=2}^{\infty}\frac{2}{\kappa\sigma_n}\exp(-\sigma_n\xi)\cos(n\pi\eta)}_{\text{Developing component}}\\ \Delta=\underbrace{\frac{1}{\mathrm{Bi}(1+\kappa)}\left[1-\frac{\cosh(\lambda(1-\eta))}{\cosh(\lambda)}\right]}_{\text{Fully developed component}}\\ \quad -[D_5\exp(-\omega_{A0}\xi)+D_6\exp(-\omega_{A1}\xi)+D_7\exp(-\sigma_1\xi)]\sin(0.5\pi\eta)\\ \quad -[D_8\exp(-\omega_{A0}\xi)+D_9\exp(-\omega_{A1}\xi)]\sin(1.5\pi\eta)\\ \quad \underbrace{-\frac{1+\kappa}{\kappa}\sum_{m=2}^{\infty}\frac{j_{m,0}}{\gamma_m}\exp(-\gamma_m\xi)\sin((0.5+m)\pi\eta)}_{\text{Developing component}}\end{cases} \tag{31}$$

where

$$\omega_{A0}=\left(B-\sqrt{B^2-4AC}\right)/2A,\quad \omega_{A1}=\left(B+\sqrt{B^2-4AC}\right)/2A \tag{32}$$

$$A = \left(1 - j_{1,0}^2 - j_{1,1}^2\right)\gamma_0 + \left(1 - j_{0,1}^2 - j_{0,0}^2\right)\gamma_1 + \left(1 - j_{1,0}^2 - j_{0,0}^2\right)\sigma_1$$
$$B = \left(1 - j_{1,0}^2\right)\sigma_1\gamma_0 + \left(1 - j_{0,0}^2\right)\sigma_1\gamma_1 + \gamma_1\gamma_0$$
$$C = \sigma_1\gamma_0\gamma_1 \tag{33}$$

and

$$D_1 = \frac{1}{\kappa A(\omega_{A1} - \omega_{A0})}\left[-\frac{\sigma_1\gamma_0\gamma_1}{\omega_{A0}^2} + \frac{1}{\omega_{A0}}(\sigma_1\gamma_0 + \sigma_1\gamma_1 + \gamma_0\gamma_1) - E_1\right]$$
$$D_2 = \frac{1}{\kappa A(\omega_{A1} - \omega_{A0})}\left[\frac{\sigma_1\gamma_0\gamma_1}{\omega_{A1}^2} - \frac{1}{\omega_{A1}}(\sigma_1\gamma_0 + \sigma_1\gamma_1 + \gamma_0\gamma_1) + E_1\right]$$
$$D_3 = \frac{1}{\kappa A(\omega_{A1} - \omega_{A0})}\left(\frac{2\gamma_0\gamma_1}{\omega_{A0}} - E_2\right)$$
$$D_4 = \frac{1}{\kappa A(\omega_{A1} - \omega_{A0})}\left(-\frac{2\gamma_0\gamma_1}{\omega_{A1}} + E_2\right)$$
$$D_5 = \frac{1+\kappa}{\kappa A(\omega_{A1} - \omega_{A0})}\left(\frac{\sqrt{2}j_{0,0}\sigma_1\gamma_1}{\omega_{A0}} - E_3 - \frac{2j_{0,1}\sigma_1\gamma_1 - \omega_{A0}E_4}{\sigma_1 - \omega_{A0}}\right)$$
$$D_6 = \frac{1+\kappa}{\kappa A(\omega_{A1} - \omega_{A0})}\left(-\frac{\sqrt{2}j_{0,0}\sigma_1\gamma_1}{\omega_{A1}} + E_3 - \frac{2j_{0,1}\sigma_1\gamma_1 - \omega_{A1}E_4}{\sigma_1 - \omega_{A0}}\right)$$
$$D_7 = \frac{\sigma_1(1+\kappa)(-2j_{0,1}\gamma_1 + E_4)}{\kappa A(\sigma_1 - \omega_{A0})(\sigma_1 - \omega_{A1})}$$
$$D_8 = \frac{1+\kappa}{\kappa A(\omega_{A1} - \omega_{A0})}\left(\frac{\sqrt{2}j_{1,0}\sigma_1\gamma_0}{\omega_{A0}} - E_5\right)$$
$$D_9 = \frac{1+\kappa}{\kappa A(\omega_{A1} - \omega_{A0})}\left(-\frac{\sqrt{2}j_{1,0}\sigma_1\gamma_0}{\omega_{A1}} + E_5\right) \tag{34}$$

$$E_1 = \sigma_1 + \gamma_0\left[\left(1 - j_{1,1}^2\right) + \sqrt{2}j_{1,0}j_{1,1}\right] + \gamma_1\left[\left(1 - j_{0,1}^2\right) + \sqrt{2}j_{0,0}j_{0,1}\right]$$
$$E_2 = \gamma_0\left[2\left(1 - j_{1,0}^2\right) + \sqrt{2}j_{1,0}j_{1,1}\right] + \gamma_1\left[2\left(1 - j_{0,0}^2\right) + \sqrt{2}j_{0,0}j_{0,1}\right]$$
$$E_3 = \sqrt{2}j_{0,0}\left[\sigma_1\left(1 - j_{1,0}^2\right) + \gamma_1\right] + \sqrt{2}j_{0,0}j_{1,0}^2\sigma_1$$
$$E_4 = 2j_{0,1}\left[\sigma_1\left(1 - j_{1,0}^2\right) + \gamma_1\right] + 2j_{0,0}j_{1,1}j_{1,0}\sigma_1$$
$$E_5 = \sqrt{2}j_{1,0}\left[\sigma_1\left(1 - j_{1,0}^2\right) + \gamma_0\right] + \sqrt{2}j_{0,0}^2j_{1,0}\sigma_1 \tag{35}$$

When removing more high ordered components as shown in Eqs. (28)–(30), some detailed information near the entrance will get lost. Hence, the approximate solution predicts less accurately near the entrance, but it still can predict accurate results in the thermally developing region.

The corresponding exact solution for thermally fully developed flow is given by Yang and Vafai [15]:

$$\begin{cases} \theta_{a,ed} = \frac{\xi}{\kappa} + \frac{(1-\eta)^2 - 1/3}{2(1+\kappa)} + \frac{1}{\mathrm{Bi}(1+\kappa)^2}\left[1 - \frac{\tanh(\lambda)}{\lambda}\right] \\ \quad = \frac{\xi}{\kappa} + \frac{(1-\eta)^2 - 1/3}{2(1+\kappa)} + \sum_{m=0}^{\infty}\frac{j_{m,0}^2}{\kappa\gamma_m} \\ \Delta_{ed} = \frac{1}{\mathrm{Bi}(1+\kappa)}\left[1 - \frac{\cosh(\lambda(1-\eta))}{\cosh(\lambda)}\right] \end{cases} \tag{36}$$

The fully developed component of Eq. (31) is quite close to the exact expressions given by Eq. (36) but misses few terms in the fully developed component part of the expression for θ_a.

3.3. Exact solution for Models B and C

Eqs. (9) and (10) for Models B and C can be expressed as

$$-\kappa\frac{\partial\theta_f}{\partial\eta} = \beta_f, \quad -\frac{\partial\theta_s}{\partial\eta} = \beta_s \quad \text{at } \eta = 0 \tag{37}$$

where $\beta_f = \beta_s = 1$ for Model B, and $\beta_f = \varepsilon$ and $\beta_s = 1 - \varepsilon$ for Model C. As such the solutions for Models B and C can be obtained simultaneously based on Eq. (37). Again, with the transformation given by Eq. (12), the governing equations and the boundary conditions given by Eqs. (11) and (37) become

$$\begin{cases} \frac{\partial\theta_a}{\partial\xi} = \frac{1+\kappa}{\kappa}\frac{\partial^2\theta_a}{\partial\eta^2} + \frac{1}{1+\kappa}\frac{\partial\Delta}{\partial\xi} \\ 0 = \frac{\partial^2\Delta}{\partial\eta^2} + \frac{1+\kappa}{\kappa}\frac{\partial^2\theta_a}{\partial\eta^2} - \mathrm{Bi}\frac{1+\kappa}{\kappa}\Delta \end{cases} \tag{38}$$

$$\begin{cases} -(1+\kappa)\frac{\partial\theta_a}{\partial\eta} = \beta_s + \beta_f, \quad -\kappa\frac{\partial\Delta}{\partial\eta} = \kappa\beta_s - \beta_f \quad \text{at } \eta = 0 \\ \frac{\partial\theta_a}{\partial\eta} = \frac{\partial\Delta}{\partial\eta} = 0 \quad \text{at } \eta = 1 \\ (1+\kappa)\theta_a = \Delta = \frac{\beta_s\cosh\left(\sqrt{\mathrm{Bi}}(1-\eta)\right)}{\sqrt{\mathrm{Bi}}\sinh\left(\sqrt{\mathrm{Bi}}\right)} \quad \text{at } \xi = 0 \end{cases} \tag{39}$$

Utilizing a series representation for θ_a and Δ as

$$\begin{cases} \theta_a = c_{\theta,0}(\xi) + \sum_{n=1}^{\infty} c_{\theta,n}(\xi)\cos(n\pi\eta) \\ \Delta = c_{\Delta,0}(\xi) + \sum_{n=1}^{\infty} c_{\Delta,n}(\xi)\cos(n\pi\eta) \end{cases} \tag{40}$$

The governing equations given by Eq. (38) can be integrated with respect to η after multiplying it by $\cos(n\pi\eta)$

$$\begin{cases} \frac{dc_{\theta,0}}{d\xi} = \frac{\beta_s+\beta_f}{\kappa} + \frac{1}{1+\kappa}\frac{dc_{\Delta,0}}{d\xi}, \quad n = 0 \\ 0 = \beta_s - \mathrm{Bi}c_{\Delta,0}, \quad n = 0 \\ \frac{dc_{\theta,n}}{d\xi} = \frac{2(\beta_s+\beta_f)}{\kappa} - \frac{1+\kappa}{\kappa}(n\pi)^2 c_{\theta,n} + \frac{1}{1+\kappa}\frac{dc_{\Delta,n}}{d\xi}, \quad n = 1,2,3,\ldots \\ 0 = 2\beta_s\frac{1+\kappa}{\kappa} - \frac{1+\kappa}{\kappa}(n\pi)^2 c_{\theta,n} - \left[(n\pi)^2 + \mathrm{Bi}\frac{1+\kappa}{\kappa}\right]c_{\Delta,n}, \quad n = 1,2,3,\ldots \end{cases} \tag{41}$$

Thus, after solving Eq. (41), the coefficients for Eq. (40) are obtained as

$$\begin{cases} c_{\theta,0} = \frac{\beta_f+\beta_s}{\kappa}\xi + \frac{\beta_s}{\mathrm{Bi}(1+\kappa)}, \quad n = 0 \\ c_{\Delta,0} = \frac{\beta_s}{\mathrm{Bi}}, \quad n = 0 \\ c_{\theta,n} = -d_{\theta,n}\exp(-\omega_{B\ or\ C,\ n}\xi) + \frac{2}{\kappa\sigma_n}, \quad n = 1,2,3,\ldots \\ c_{\Delta,n} = -d_{\Delta,n}\exp(-\omega_{B\ or\ C,\ n}\xi) + \frac{\kappa\beta_s - \beta_f}{\kappa[(n\pi)^2 + \lambda^2]}, \quad n = 1,2,3,\ldots \end{cases} \tag{42}$$

where

$$\omega_{B\ or\ C,\ n} = \frac{(n\pi)^2\left[(n\pi)^2 + \lambda^2\right]}{(n\pi)^2 + \mathrm{Bi}} \tag{43}$$
$$d_{\theta,n} = \frac{2(\beta_f + \beta_s)}{\kappa\sigma_n} - \frac{2\beta_s/(1+\kappa)}{(n\pi)^2 + \mathrm{Bi}} \tag{44}$$
$$d_{\Delta,n} = \frac{\kappa\beta_s - \beta_f}{\kappa[(n\pi)^2 + \lambda^2]} - \frac{2\beta_s}{(n\pi)^2 + \mathrm{Bi}} \tag{45}$$

The exact solutions for Models B and C can be expressed as

$$\begin{cases} \theta_a = \underbrace{\frac{\beta_f+\beta_s}{\kappa}\xi + \frac{\beta_f+\beta_s}{2(1+\kappa)}[(1-\eta)^2 - 1/3] + \frac{\beta_s}{(1+\kappa)\mathrm{Bi}}}_{\text{Fully developed component}} \\ \quad \underbrace{-\sum_{n=1}^{\infty} d_{\theta,n}\exp(-\omega_{B\ or\ C,\ n}\xi)\cos(n\pi\eta)}_{\text{Developing component}} \\ \Delta = \underbrace{\frac{\beta_f+\beta_s}{(1+\kappa)\mathrm{Bi}} + \frac{\kappa\beta_s - \beta_f}{\kappa\lambda}\frac{\cosh(\lambda(1-\eta))}{\sinh(\lambda)}}_{\text{Fully developed component}} \underbrace{-\sum_{n=1}^{\infty} d_{\Delta,n}\exp(-\omega_{B\ or\ C,\ n}\xi)\cos(n\pi\eta)}_{\text{Developing component}} \end{cases} \tag{46}$$

The fully developed component in Eq. (46) is the same as the corresponding exact solution for thermally fully developed flow given by Yang and Vafai [15].

3.4. Exact solution for the LTE model

The governing equation for the LTE model can be obtained by assuming that the temperatures of the fluid and solid phases are the same in Eq. (7). That is

$$\kappa\frac{\partial\theta}{\partial\xi}=(\kappa+1)\frac{\partial^2\theta}{\partial\eta^2} \tag{47}$$

The boundary conditions for the LTE model is represented by

$$\begin{cases}-(\kappa+1)\frac{\partial\theta}{\partial\eta}=1 \text{ at } \eta=0\\ \frac{\partial\theta}{\partial\eta}=0 \quad \text{at } \eta=1\\ \theta=0 \quad \text{at } \xi=0\end{cases} \tag{48}$$

The exact solution can be obtained as

$$\theta=\underbrace{\frac{\xi}{\kappa}+\frac{(1-\eta)^2-1/3}{2(1+\kappa)}}_{\text{Fully developed component}}\underbrace{-\sum_{n=1}^{\infty}\frac{2}{\kappa\sigma_n}\exp(-\sigma_n\xi)\cos(n\pi\eta)}_{\text{Developing component}} \tag{49}$$

Within all these analytical results, it should be noted that there are two aspects that are consistent with all of the solutions when Bi $\to\infty$: First, the θ_a's based on LTNE model for Models A, B and C in Eqs. (31) and (46) approach the θ based on LTE model in Eq. (49). Second, the Δ's in Eqs. (31) and (46) approach 0. Thus, all these analytical solutions for the LTNE model are consistent with the solution for the LTE model.

4. Validation and comparisons

4.1. Nussuelt number results

The local Nusselt number for Model A is defined as

$$\mathrm{Nu}(\xi)=\frac{q_w(4H)}{k_{f,eff}\left(\frac{k_{f,eff}T_f+k_{s,eff}T_s}{k_{f,eff}+k_{s,eff}}\Big|_{y=0}-\frac{1}{H}\int_0^H T_f dy\right)}=\frac{4}{\kappa\theta_a|_{\eta=0}-\xi} \tag{50}$$

As expected and seen in Fig. 2, Nu decreases along with the axial coordinate at first and then approaches a constant value. The transition point is $\xi=\xi_c$ where the flow can be recognized as thermally fully developed.

Fig. 2 shows the local Nusselt number comparisons between the approximate solution and the numerical solution for Model A. The approximate solution diverges slightly from the numerical solution for lower values of κ and Bi. The approximate solution agrees very well with the numerical solution in the range of κ and Bi given by $\kappa>0.01$ and Bi > 0.1.

For Models B and C, the local Nusselt number is defined as

$$\mathrm{Nu}(\xi)=\frac{4(\beta_f+\beta_s)}{\kappa\theta_a|_{\eta=0}-\xi(\beta_f+\beta_s)} \tag{51}$$

Fig. 3 displays the Nusselt number distributions for Models B and C for $\varepsilon=0.8$ based on the obtained exact solution and the numerical solution. As it can be seen there is perfect agreement between the two solutions. In contrast to Model A, the Nusselt number distribution curves for Models B and C become substantially flatter as Bi decreases. For example, for Model B with $\kappa=0.1$ and Bi = 0.1, the Nusselt number at the inlet is not much different from that in the fully developed region, as seen in Fig. 3. This demonstrates that the thermally developing effects have a negligible influence on the local Nussult number for Models B and C for lower values of the Biot number.

The primary reason for this effect is that Models B and C utilize a constant heat flux on the solid phase boundary. It should be noted that for Models B and C the heat received by the solid phase has to transfer to the fluid phase by the internal convection in porous media [15–17]. As shown in Fig. 4(a), for lower values of the Biot number such as Bi = 0.1, θ_s is much higher than θ_f at every point in the channel for Model B. As a result, θ_s is not influenced by the thermal boundary effects of the fluid phase. Thus, the local Nusselt number does not show the thermally developing effects for such a case. Fig. 4(b) shows another case with Bi = 10 for Model B where θ_s is of the same order of magnitude as θ_f. Thus, the thermally developing effects are significant. However, for Model A even for low values of Bi, the imposed condition of $\theta_f=\theta_s$ ensures that θ_s and θ_f have the same order of magnitude near the heated wall, where the thermal boundary effects can be important, as shown in Fig. 4(c). Therefore, the local Nusselt number will always display the thermal developing effects for Model A.

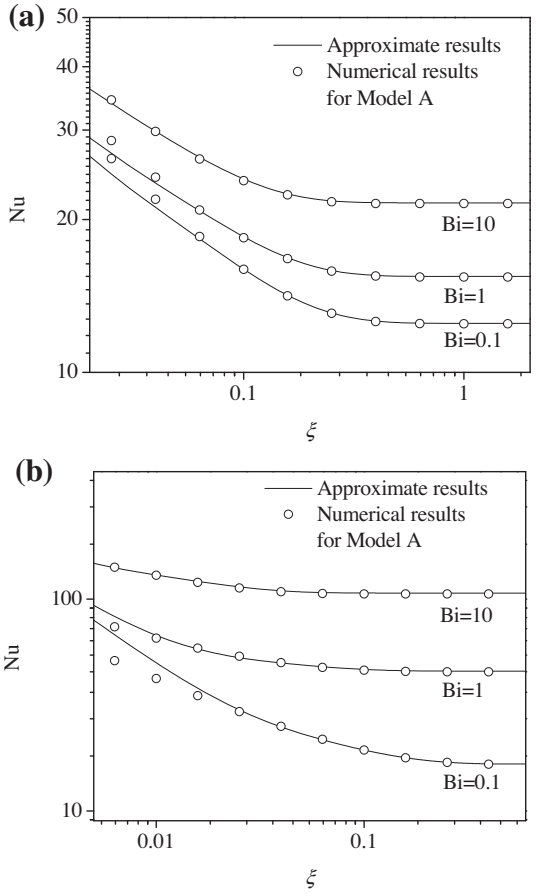

Fig. 2. Local Nusselt number distributions for Model A for: (a) $\kappa=1$, (b) $\kappa=0.1$.

4.2. Predictions of the thermal entry length

The classical definition for thermal entry length is based on the local Nusselt number. The dimensionless thermal entry length ξ_c is defined as

$$\frac{\mathrm{Nu}(\xi)-\mathrm{Nu}_{ed}}{\mathrm{Nu}_{ed}}=1\%, \quad \text{at } \xi=\xi_c \tag{52}$$

where Nu_{ed} is the Nusselt number for the fully developed section. That is

$$\mathrm{Nu}_{ed}=\mathrm{Nu}(\xi), \quad at\ \xi\to\infty \tag{53}$$

Combining the definitions for ξ_c and Nu, i. e., Eqs. (52), (50) and (51), and utilizing the presented analytical solutions, an explicit expression for ξ_c can be derived for Models A, B and C, as follows:

For Model A:

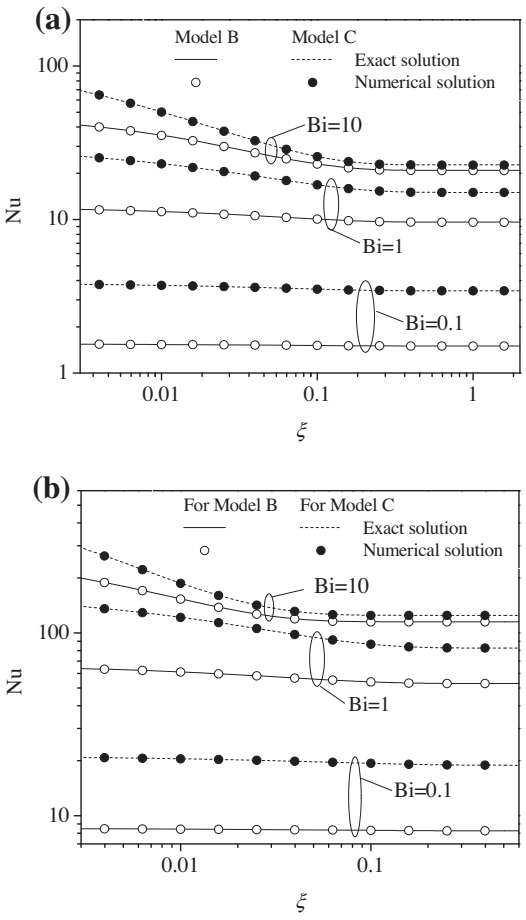

Fig. 3. Local Nusselt number distributions for Model B and Model C with $\varepsilon = 0.8$ for: (a) $\kappa = 1$, (b) $\kappa = 0.1$.

$$\frac{1}{1+\frac{\mathrm{Nu}_{ed}}{\mathrm{Nu}(\xi_c)-\mathrm{Nu}_{ed}}} = \frac{(D_1+D_3)\exp(-\omega_{A0}\xi_c)+(D_2+D_4)\exp(-\omega_{A1}\xi_c)+\sum_{n=2}^{\infty}\frac{2}{\kappa\sigma_n}\exp(-\sigma_n\xi_c)}{\frac{1}{3(1+\kappa)}+\frac{j_{0,0}^2}{\kappa\gamma_0}+\frac{j_{1,0}^2}{\kappa\gamma_1}} \approx \frac{6}{\pi^2}f_A\exp(-\omega_{A0}\xi_c) \tag{54}$$

And for Models B and C:

$$\frac{1}{1+\frac{\mathrm{Nu}_{ed}}{\mathrm{Nu}(\xi_c)-\mathrm{Nu}_{ed}}} = \frac{\sum_{n=1}^{\infty}d_{\theta,n}\exp(-\omega_{B\ or\ C,\ n}\xi_c)}{\frac{\beta_f+\beta_s}{3(1+\kappa)}+\frac{\beta_s}{(1+\kappa)\mathrm{Bi}}} \approx \frac{6}{\pi^2}f_{B\ or\ C}\exp(-\omega_{B\ or\ C,\ 1}\xi_c) \tag{55}$$

while for the LTE model:

$$\frac{1}{1+\frac{\mathrm{Nu}_{ed}}{\mathrm{Nu}(\xi_c)-\mathrm{Nu}_{ed}}} = \frac{\sum_{n=1}^{\infty}\frac{2}{\kappa\sigma_n}\exp(-\sigma_n\xi_c)}{\frac{1}{3(1+\kappa)}} \approx \frac{6}{\pi^2}f_{LTE}\exp(-\sigma_1\xi_c) \tag{56}$$

It is found that only the largest term dominates the series in Eqs. (54)–(56). As such the approximate form of ξ_c can be found from Eqs. (54)–(56) as follows:

$$\xi_c = \frac{\kappa\ln(61.4f_i)}{\pi^2(1+\kappa)}\chi_i \tag{57}$$

where χ_i and f_i are the correction functions for the LTNE model presented below, and the subscript i denotes different models that were considered before, that is $i = A, B, C$, or LTE:

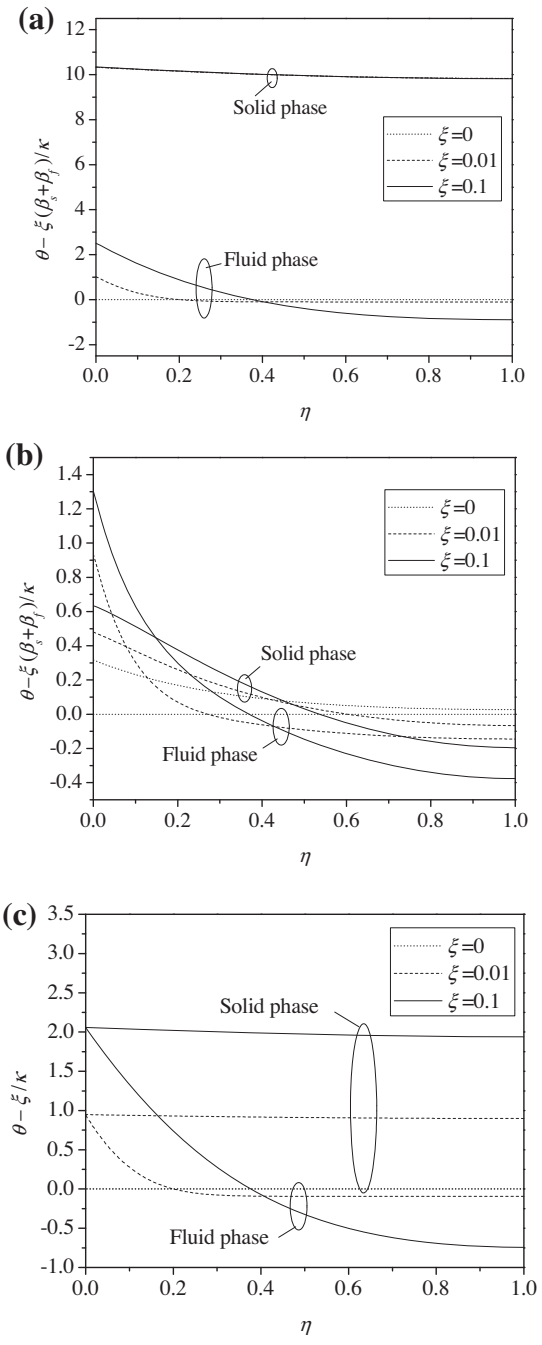

Fig. 4. Dimensionless temperature distributions at different cross sections of the channel for: (a) Model B for $\kappa = 0.1$ and $\mathrm{Bi} = 0.1$, (b) Model B for $\kappa = 0.1$ and $\mathrm{Bi} = 10$, (c) Model A for $\kappa = 0.1$ and $\mathrm{Bi} = 0.1$.

$$\chi_i = \begin{cases} \chi_A = \sigma_1/\omega_{A0} \\ \chi_{B\ or\ C} = \left(\frac{\mathrm{Bi}}{\mathrm{Bi}+\pi^2}+\kappa\right)/(1+\kappa) \\ \chi_{LTE} = 1 \end{cases} \tag{58}$$

$$f_i = \begin{cases} f_A = \frac{\pi^2}{6}(D_1+D_3)\Big/\left[\frac{1}{3(1+\kappa)}+\frac{j_{0,0}^2}{\kappa\gamma_0}+\frac{j_{1,0}^2}{\kappa\gamma_1}\right] \\ f_{B\ or\ C} = \frac{\pi^2}{6}\left[\frac{2}{\pi^2}+\frac{2\beta_s/(\beta_s+\beta_f)}{\pi^2+\mathrm{Bi}}\right]\Big/\left[\frac{1}{3}+\frac{\beta_s/(\beta_s+\beta_f)}{\mathrm{Bi}}\right] \\ f_{LTE} = 1 \end{cases} \tag{59}$$

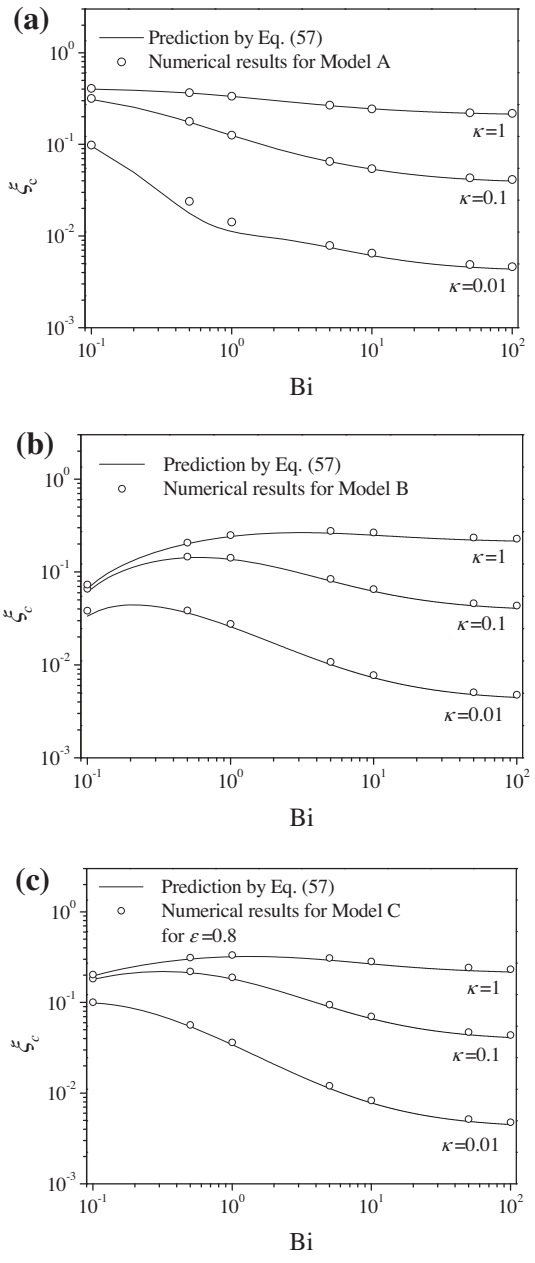

Fig. 5. Dimensionless thermal entry length and its comparison with the numerical results for: (a) Model A, (b) Model B, (c) Model C for $\varepsilon = 0.8$.

As shown in Eqs. (57)–(59), ξ_c is a function of Bi, κ and the boundary condition models. It should be noted that if Bi $\to \infty$, then $\chi_i \to 1$ and $f_i \to 1$, because Bi $\to \infty$ represents the LTE condition.

The comparisons between the analytical expressions for ξ_c given by Eq. (57) and the numerical results are shown in Fig. 5. As can be seen the analytical and numerical results are in excellent agreement. It can be seen in Fig. 5(a), for Model A that ξ_c increases as κ increases or Bi decreases. However, for Models B and C, ξ_c is non-monotonic with Bi, as seen in Fig. 5(b) and (c). The reason for this behavior has been discussed earlier in Section 4.1.

5. Conclusions

In the present work, analytical solutions for thermally developing flow in porous media incorporating LTNE condition are derived for different fundamental models. A highly accurate approximate solution for Model A, and exact solution for Models B and C are established. These analytical solutions are in excellent agreement with the numerical results. For Models B and C, the thermal developing effects are found to be negligible for lower values of the Biot numbers.

The dimensionless thermal entry length ξ_c is established based on the analytical solutions and it is found to be a function of the Biot Number, Bi, the ratio of fluid to solid conductivity, κ as well as a function of models A, B and C. For Model A, ξ_c increases as κ increases or Bi decreases. But for Models B and C, ξ_c is non-monotonic with Bi.

The present work paves the way for understanding and designing the thermally developing flows in porous media while incorporating the LTNE condition.

Acknowledgements

This project was supported by the National Natural Science Foundation of China (Grant No. 51276094) and the Key Project Fund of the National Natural Science Foundation of China (No. 50736003). We would also like to acknowledge the financial support from China Scholarship Council.

References

[1] A. Bejan, Convection Heat Transfer, Wiley, New York, 2004.
[2] K. Vafai, C.L. Tien, Boundary and inertia effects on flow and heat transfer in porous media, Int. J. Heat Mass Transfer 24 (2) (1981) 195–203.
[3] A. Haji-Sheikh, K. Vafai, Analysis of flow and heat transfer in porous media imbedded inside various-shaped ducts, Int. J. Heat Mass Transfer 47 (8) (2004) 1889–1905.
[4] A. Haji-Sheikh, D.A. Nield, K. Hooman, Heat transfer in the thermal entrance region for flow through rectangular porous passages, Int. J. Heat Mass Transfer 49 (17) (2006) 3004–3015.
[5] A. Amiri, K. Vafai, Analysis of dispersion effects and non-thermal equilibrium, non-Darcian, variable porosity incompressible flow through porous media, Int. J. Heat Mass Transfer 37 (6) (1994) 939–954.
[6] P.X. Jiang, Z.P. Ren, B.X. Wang, Numerical simulation of forced convection heat transfer in porous plate channels using thermal equilibrium and nonthermal equilibrium models, Numer. Heat Transfer: Part A: Appl. 35 (1) (1999) 99–113.
[7] P.X. Jiang, M. Li, Y.C. Ma, Z.P. Ren, Boundary conditions and wall effect for forced convection heat transfer in sintered porous plate channels, Int. J. Heat Mass Transfer 47 (10) (2004) 2073–2083.
[8] P.X. Jiang, Z. Wang, Z.P. Ren, B.X. Wang, Experimental research of fluid flow and convection heat transfer in plate channels filled with glass or metallic particles, Exp. Thermal Fluid Sci. 20 (1) (1999) 45–54.
[9] P.X. Jiang, M. Li, T.J. Lu, L. Yu, Z.P. Ren, Experimental research on convection heat transfer in sintered porous plate channels, Int. J. Heat Mass Transfer 47 (10) (2004) 2085–2096.
[10] D.A. Nield, A.V. Kuznetsov, Forced convection in porous media: transverse heterogeneity effects and thermal development, in: Handbook of Porous Media, second ed., Taylor and Francis, New York, 2005, pp. 143–193.
[11] K. Yang, K. Vafai, Transient aspects of heat flux bifurcation in porous media: an exact solution, J. Heat Transfer 133 (5) (2011) 052602.
[12] B. Alazmi, K. Vafai, Constant wall heat flux boundary conditions in porous media under local thermal non-equilibrium conditions, Int. J. Heat Mass Transfer 45 (15) (2002) 3071–3087.
[13] X.L. Ouyang, P.X. Jiang, R.N. Xu, Thermal boundary conditions of local thermal non-equilibrium model for convection heat transfer in porous media, Int. J. Heat Mass Transfer 60 (2013) 31–40.
[14] D.Y. Lee, K. Vafai, Analytical characterization and conceptual assessment of solid and fluid temperature differentials in porous media, Int. J. Heat Mass Transfer 42 (3) (1999) 423–435.
[15] K. Yang, K. Vafai, Analysis of temperature gradient bifurcation in porous media – An exact solution, Int. J. Heat Mass Transfer 53 (19) (2010) 4316–4325.
[16] K. Yang, K. Vafai, Restrictions on the validity of the thermal conditions at the porous-fluid interface – An exact solution, J. Heat Transfer 133 (2011) 112601.
[17] K. Yang, K. Vafai, Analysis of heat flux bifurcation inside porous media incorporating inertial and dispersion effects – An exact solution, Int. J. Heat Mass Transfer 54 (2011) 5286–5297.
[18] A. Amiri, K. Vafai, T.M. Kuzay, Effects of boundary-conditions on non-Darcian heat transfer through porous media and experimental comparisons, Numer. Heat Transfer A Appl. 27 (6) (1995) 651–664.